



Published in final edited form as:

Radiother Oncol. 2023 June ; 183: 109641. doi:10.1016/j.radonc.2023.109641.

Prospective validation of diffusion-weighted MRI as a biomarker of tumor response and oncologic outcomes in head and neck cancer: Results from an observational biomarker pre-qualification study

Joint Head and Neck Radiotherapy-MRI Development Cooperative

Abdallah S. R. Mohamed, MD, PhD^{1,3}, Abdelrahman Abusaif, MD¹, Renjie He, PhD¹, Kareem Wahid, BS^{1,3}, Vivian Salama, MD, MSc^{1,3}, Sara Youssef, BS¹, Brigid A. McDonald, PhD^{1,3}, Mohamed Naser, PhD¹, Yao Ding, PhD¹, Travis C. Salzillo, PhD¹, Moamen A. AboBakr, MD¹, Jihong Wang, PhD¹, Stephen Y. Lai, MD, PhD^{1,2,3,*}, Clifton D. Fuller, MD, PhD^{1,3,*}

¹Department of Radiation Oncology, The University of Texas, MD Anderson Cancer Center, Houston, TX, USA.

²Department of Head and Neck Surgery, The University of Texas, MD Anderson Cancer Center, Houston, TX, USA.

³The University of Texas MD Anderson Cancer Center UTHealth Graduate School of Biomedical Sciences.

Abstract

Purpose: To determine DWI parameters associated with tumor response and oncologic outcomes in head and neck (HNC) patients treated with radiotherapy (RT).

Methods: HNC patients in a prospective study were included. Patients had MRIs pre-, mid-, and post-RT completion. We used T2-weighted sequences for tumor segmentation which were co-registered to respective DWIs for extraction of apparent diffusion coefficient (ADC) measurements. Treatment response was assessed at mid- and post-RT and was defined as: complete response (CR) vs. non-complete response (non-CR). The Mann-Whitney U test was used to compare ADC between CR and non-CR. Recursive partitioning analysis (RPA) was performed to identify ADC threshold associated with relapse. Cox proportional hazards models were done for clinical vs. clinical and imaging parameters and internal validation was done using bootstrapping technique.

Results: Eighty-one patients were included. Median follow-up was 31 months. For patients with post-RT CR, there was a significant increase in mean ADC at mid-RT compared to baseline ((1.8

*Co-corresponding Author: Stephen Y. Lai, MD, PhD, Department of Head and Neck Surgery, The University of Texas- MD Anderson Cancer Center, Houston, TX, USA. sylai@mdanderson.org, Clifton D. Fuller, MD, PhD, Department of Radiation Oncology, The University of Texas- MD Anderson Cancer Center, Houston, TX, USA. cdfuller@mdanderson.org.

Conflict of interest statement: The authors declare no conflicts of interest.

Publisher's Disclaimer: This is a PDF file of an unedited manuscript that has been accepted for publication. As a service to our customers we are providing this early version of the manuscript. The manuscript will undergo copyediting, typesetting, and review of the resulting proof before it is published in its final form. Please note that during the production process errors may be discovered which could affect the content, and all legal disclaimers that apply to the journal pertain.

$\pm 0.29) \times 10^{-3} \text{ mm}^2/\text{s}$ vs. $(1.37 \pm 0.22) \times 10^{-3} \text{ mm}^2/\text{s}$, $p < 0.0001$), while patients with non-CR had no significant increase ($p > 0.05$). RPA identified GTV-P delta (Δ) $\Delta\text{ADC}_{\text{mean}} < 7\%$ at mid-RT as the most significant parameter associated with worse LC and RFS ($p = 0.01$). Uni- and multi-variable analysis showed that GTV-P $\Delta\text{ADC}_{\text{mean}}$ at mid-RT $> 7\%$ was significantly associated with better LC and RFS. The addition of $\Delta\text{ADC}_{\text{mean}}$ significantly improved the c-indices of LC and RFS models compared with standard clinical variables (0.85 vs. 0.77 and 0.74 vs. 0.68 for LC and RFS, respectively, $p < 0.0001$ for both).

Conclusion: $\Delta\text{ADC}_{\text{mean}}$ at mid-RT is a strong predictor of oncologic outcomes in HNC. Patients with no significant increase of primary tumor ADC at mid-RT are at high risk of disease relapse.

Introduction

Radiation therapy (RT) is a cornerstone of head and neck cancer (HNC) treatment both in the definitive (i.e., organ preserving) and adjuvant post-operative setting. The goal of RT is to maximize the dose to cancer cells while minimizing the dose to adjacent normal tissues. However, tumors have variable sensitivity to RT leading to different disease response rates.[1] Current RT dose and fractionation are largely driven by empirical data rather than tumor-specific information regarding potential radiosensitivity or radioresistance.[2–5] The ability to predict tumor response before and/or during the RT course can allow for the adaptation of RT doses and potentially achieve better treatment outcomes for patients.

Non-invasive imaging such as magnetic resonance imaging (MRI) can provide important information related to tumor characteristics and response to RT. The development of MRI correlates of RT response would be critical for implementing adaptive RT strategies that maximize therapeutic ratios. Specifically, patients with aggressive non-responsive tumors may require RT dose escalation [3, 5], while patients with radiosensitive tumors may benefit from dose de-escalation to spare normal tissues with equivalent tumor control.[4] This represents a significant unmet clinical need since patients with radiosensitive tumors are over-treated and patients with radio-resistant tumors are under-treated. A leading-edge solution to the anatomic adaptive therapy problem has been to integrate MRI into radiation delivery devices (e.g., MR-Linear accelerators).[6] The richer data of MRI compared with standard-of-care CT images enables computer-driven identification of tumors and normal tissues and allows radiation plans to be adapted on a daily basis with limited human intervention. [7, 8] Yet, gross anatomic changes represent only one dimension of patient response to RT. Having incorporated high-field MRI into delivery devices, there is now the potential to monitor the biologic changes within the patient using quantitative MRI sequences without excess radiation, contrast exposure, or excess burden on patients' time.

The central hypothesis of this study is that quantitative MR diffusion-weighted imaging (DWI) can be used as a predictive biomarker of treatment response and oncologic outcomes in HNC. Functional changes in a tissue (e.g., a reduction in cellular density through RT-induced apoptosis) is reflected in an alteration in the detected diffusion measures, using a metric known as the apparent diffusion coefficient (ADC). The ADC component of DWI has been previously used to detect treatment response in HNC.[9–11] Specifically, DWI has been shown to predict response to induction chemotherapy[12, 13], RT[11, 13–20],

and tumor recurrence[21]. Preliminary data from a prospective trial at our institution[22], supported by other group's data[13, 15–17, 20, 23, 24], has demonstrated that DWI was able to discriminate patients who will have a complete response at mid-RT. Additionally, recent data from our group demonstrated that early tumor regression rate 25% at fraction 15 (i.e., mid-RT) in HNC patients is associated with better local control and overall survival.[25] These low-risk patients represent suitable candidates for RT dose de-escalation if dose could be coupled to a quantitative marker of tumor response probability (i.e., ADC). However, these findings remain to be validated in larger prospective studies with more mature follow-up data to correlate with oncologic outcomes and overall survival. To this end, we aim to determine DWI parameters associated with tumor response and oncologic outcomes in a prospective cohort of HNC patients treated with definitive RT.

Methods

Patient selection

HNC patients enrolled in an active prospective imaging study (NCT03145077) from January 2017 to March 2021 were included after institutional-review board approval and study-specific informed consent. Patients in this cohort had MRIs at pre-RT, mid-RT, and post-RT. Inclusion criteria were adult patients with histologic evidence of malignant head and neck neoplasm obtained from the primary tumor or metastatic lymph node; indicated for curative-intent treatment with radiotherapy with or without chemotherapy (induction or concurrent); good performance status (ECOG score 0–2); and with no contraindications to MRI. Patients evaluated in this study received RT using standard daily fractionation for a period of 6–7 weeks. Tumor staging was based on clinical imaging consisting of contrast (CE) CT prior to treatment initiation using current AJCC 8th edition staging criteria.

MR Imaging

All patients enrolled in the study had imaging acquired using individualized immobilization devices. Head immobilization was performed to decrease motion artifacts during the imaging study, according to the methodology presented previously by our group.[26] Patients were scanned using a MAGNETOM Aera 1.5T MR scanner (Siemens Healthcare, Erlangen, Germany) with two large four-channel flex phased-array coils. After the scout scan, an anatomic T2-weighted (T2w) fast spin-echo sequence (TR/TE = 4.8 s/80 ms; echo train length = 15, pixel bandwidth = 300 Hz, slice thickness = 2 mm, matrix = 512 × 512) was performed. 120 axial slices with a field of view (FOV) of 25.6 cm were selected to cover the primary tumor and neck nodes. Acquisition parameters for DWI were multi shot radial turbo spin-echo (i.e., BLADE), axial acquisition; TR = 6.5 s; TE = 50 ms; pixel bandwidth = 1220 Hz; FOV = 25.6 × 25.6 cm²; echo train length = 15; EPI factor = 7, acquisition matrix = 128 × 128; voxel size = 1 × 1 × 2 mm³; 24 contiguous slices; two b-values = 0 and 800 (sec/mm²) for each orthogonal diffusion direction; number of averages = 2 for b=0 and 8 for b=800. DWI acquisition of patients scanned after 2018 was performed with multi-shot spin-echo echo-planar imaging (i.e. readout segmentation of long variable echo-trains, RESOLVE), axial acquisition; TR = 3.5 s; TE = 65 ms; pixel bandwidth = 780 Hz; FOV = 25.6 × 25.6 cm²; acquisition matrix = 128 × 128; slice thickness = 4 mm; reconstruction voxel size = 1 × 1 × 2 mm³, 48 contiguous slices; two b-values = 0 and

800 (sec/mm^2) for each orthogonal diffusion direction; number of averages = 2 for $b=0$ and 8 for $b=800$. ADC maps were subsequently autogenerated using a scanner-specific on-line software during image generation. RESOLVE was selected because of shorter scan time (3:30 vs. 7:03 minutes for BLADE) and relatively higher signal-to-noise ratio. Our quality assurance study using phantom, volunteer, and patient images showed that both methods display similar ADC values with no differences in repeatability studies.[27]

Image Segmentation/Registration

The regions of interest (ROIs) for the primary gross tumor volume (GTV-P) and the nodal gross tumor volume (GTV-N) were manually segmented by an expert radiation oncologist (ASRM) using the pre-RT T2w images. Deformable image registration (DIR) was used to register MR sequences at different time points (i.e., baseline and mid-RT) using the benchmarked commercially available image registration software (Velocity AI, version 3.0.1, Atlanta, GA). All baseline GTV-P ROIs were then propagated to the mid-RT T2w images (i.e., mid-RT GTV-P) which represent the same three-dimensional (3D) volume of the original GTV-P on mid-RT images and include both responding and non-responding voxels. This was followed by quality assurance (QA) review and manual editing whenever needed to exclude air gaps or non-anatomically relevant parts in case of massive tumor shrinkage. Residual GTV-N ROIs, on the other hand, were all manually segmented on mid-RT images. Subsequently, DWI images were co-registered with the corresponding T2w of each time point and finally all ROIs were propagated to extract corresponding ADC values.[28] Additional ROIs were created on mid-RT images for patients with non-complete GTV-P response at mid-RT to assess DWI differences between responding and non-responding sub-volumes within the mid-RT GTV-P based on the radiographic findings on the mid-RT T2-weighted images. The first sub-volume was labeled mid-RT GTV-P-RD which represents the residual disease and the second sub-volume was labeled mid-RT GTV-P-RS which represents the area of response. Figure 1 illustrates the workflow process for image registration and segmentation.

Outcome definition

Treatment response was assessed at mid-RT and at 8–12 weeks post-RT using RECIST 1.1 criteria and was defined as: complete response (CR) vs. non-complete response (non-CR). Supplementary Figure 1 visually illustrates examples of the radiographic response at mid-RT of a CR and a non-CR patient. All patients had complete physical examination, fiberoptic endoscopy, MRI, and CECT or FDG PET-CT performed 8–12 weeks after RT completion to assess the final treatment response. Oncologic outcomes included two-year local control (LC), regional control (RC), freedom from distant metastasis (FDM), recurrence-free survival, and overall survival.

Statistical analysis

Continuous data were presented as mean \pm standard deviation (SD), and categorical data were presented as proportions. The Kolmogorov–Smirnov test was used to assess the difference in baseline ADC in BLADE vs. RESOLVE DWI sequences. The ADC values for all voxels included in GTV-P and GTV-N ROIs were assessed by histogram analysis and the following parameters were extracted using in-house MATLAB script (MATLAB,

MathWorks, MA, USA): ADC mean, 5th, 10th, 20th, 30th, 40th, 50th (i.e. median), 60th, 70th, 80th, 90th, 95th percentile. Pre-RT ADC parameters were correlated with RT response (CR vs. non-CR) at mid- and postRT time points using the non-parametric Mann-Whitney U test to compare ADC values between the mid-RT CR and non-CR groups. The non-parametric Wilcoxon signed-rank test was used to compare the mid-RT versus baseline ADC. Delta ADC (Δ ADC) were calculated as the percent change of ADC relative to baseline value for each parameter (i.e., $\frac{midRTADC - preRTADC}{preRTADC} \times 100$). Delta volumetric changes for both GTV-P and GTV-N at mid-RT were also calculated and the non-parametric Spearman's Rho test was used to determine the relationship between Δ ADC and Δ volume changes. Recursive partitioning analysis (RPA) was performed to identify Δ ADC threshold associated with relapse. Oncologic and survival endpoints were calculated using the Kaplan-Meier method and the statistical significance was determined using a p-value <0.05. Uni- and multi-variable analyses for oncologic and survival endpoints were performed using Cox regression. For multivariable analysis, we tested the impact of including the ADC parameter of choice (i.e., with most significant correlation with relapse based on RPA) compared with baseline models of standard clinical variables. [29] We subsequently compared the new model using Bayesian information criteria (BIC).[30] A lower BIC indicates improved model performance and parsimony, using the BIC evidence grades presented by Raftery [31] with the posterior probability of superiority of a lower BIC model, where a BIC decrease of < 2 is considered "Weak" (representing a 50–75% posterior probability of being superior model), 2–6 denoted "Positive" (posterior probability of 75–95%), 6–10 as "Strong" (posterior probability of > 95%), and > 10, "Very strong" (posterior probability > 99%). In addition, Cox proportional hazards models were constructed using the scikit-survival package in Python version 3.9.7.[32] We initially constructed standard clinical models that include T stage, HPV status, and smoking status for LC prediction and AJCC stage 8th edition, age at diagnosis, and smoking status for RFS prediction. The selection of these clinical variables was based on the findings of our group's large-scale HNC clinical models' performance for survival endpoints prediction.[29] Subsequently, additive models that include the clinical parameters plus the imaging parameter of choice (i.e., based on the findings of RPA) were constructed to assess the potential additive value of the imaging parameter. Models were only constructed for patients with a GTV-P. Patients were split into training (85%) and testing (15%) sets through a bootstrap procedure (1000 iterations) for the internal validation and evaluation of constructed models. Mean and standard deviation of c-index values across all bootstrap iterations were reported for each model. Wilcoxon signed-rank tests were applied to compare clinical and additive models for each outcome. Finally, we did further confirmatory validation of the robustness of our findings by collecting an additional external independent dataset that included patients with baseline and mid-RT DWIs acquired at our institution on a standard clinical setting. We used an IRB approved retrospective imaging protocol (RCR03–0800) to collect the data (i.e. independent retrospective dataset). All other analyses were executed with JMP Pro version 15 software (SAS Institute, Cary, NC). The analysis and reporting of the results of this study adopted the reporting recommendations for tumor marker prognostic studies (REMARK) checklist.[33]

Results

Eighty-six patients were enrolled. Five patients were excluded from this analysis because of lack of visible GTVs after induction chemotherapy ($n = 3$) and loss to follow-up ($n = 2$) leaving a total of 81 patients in the final analysis. At pre-RT, 53 patients had both baseline GTV-P and GTV-N, 6 patients had baseline GTV-P without GTV-N, and 22 patients had GTV-N with no GTV-P (i.e., total GTV-P=59 and total GTV-N=74). Patients with no visible GTV-P at baseline had either carcinoma of neck nodes of unknown primary (CUP; $n=12$), tonsillectomy prior to RT ($n=6$), or CR to induction chemotherapy ($n=4$). The mean number of RT fractions received before mid-RT images was 17.6 (SD 1.9). The majority of patients were men ($n=74$, 93%) and the median age was 61 years (range 33–78). Most patients had human papillomavirus (HPV) positive disease ($n= 73$, 90%). A summary of patient demographic, disease, and treatment criteria is presented in Table 1.

The general treatment outcomes showed that for patients with GTV-P at baseline ($n=59$), 18 (31%) had mid-RT CR at the primary site which increased to 53 (90%) post-RT. Only 6 patients (10%) had persistent local disease as assessed by imaging at post-RT. Among the 6 patients, all had subsequent pathological confirmation of residual/recurrent disease. For patients with GTV-N at baseline ($n=75$), no patient had CR at the neck at mid-RT while 65 patients (87%) had CR as assessed by imaging at post-RT. Upon further pathological assessment, 6 out of 10 patients with non-CR at the neck had residual/recurrent disease while the remainder had necrotic non-active tissue.

The median follow-up time was 31 months (IQR, 18–38). The 2-year LC, RC, and FDM for the entire cohort were 91%, 92%, and 91%, respectively. The 2-year RFS and OS were 83% and 94%, respectively. The total number of recurrence events was 15 (18%). Two, three, and five patients had an isolated local, regional, and distant recurrence events, respectively. One, two, and two patients had combined local & distant, locoregional, and locoregional & distant recurrences, respectively.

Baseline mean, median, and different histogram percentile ADC values for BLADE vs. RESOLVE were not significantly different for both GTV-P and GTV-N ROIs ($p > 0.05$ for both, Figure 2). There was no statistically significant correlation between pre-RT ADC parameters and CR at mid-RT and post-RT time points for GTV-P. Similarly, there was no significant correlation between pre-RT parameters and CR at post-RT for GTV-N ($p > 0.05$ for all). Univariable analysis also did not show a significant correlation between pre-RT ADC parameters and all oncologic and survival endpoints.

There was a statistically significant increase in all mid-RT GTV-P ADC parameters compared to baseline values ($p < 0.0001$ for all, Table 2). Additionally, there was a statistically significant increase in all mid-RT GTV-N ADC parameters compared to baseline values ($p < 0.0001$ for all, Table 2). For patients with CR of the primary tumor at the end of RT, there was a significant increase in GTV-P ADC_{mean} at mid-RT compared to baseline ($(1.8 \pm 0.29) \times 10^{-3} \text{ mm}^2/\text{s}$ versus $(1.37 \pm 0.22) \times 10^{-3} \text{ mm}^2/\text{s}$, $p < 0.0001$). On the other hand, patients with non-CR had no statistically significant increase in GTV-P ADC_{mean} ($p > 0.05$). All other studied ADC parameters also had a significant increase at mid-RT for patients with CR

of the primary tumor at the end of RT compared to non-CR. However, there was a significant increase in GTV-N ADC parameters at mid-RT for both patients with CR and non-CR at the end of RT.

RPA analysis identified GTV-P $\Delta\text{ADC}_{\text{mean}} < 7\%$ at mid-RT as the most significant parameter associated with worse LC and RFS ($p=0.01$). The 2-Year LC and RFS for patients with $\Delta\text{ADC}_{\text{mean}} < 7\%$ compared to patients with $\geq 7\%$ at mid-RT were 48% and 42% versus 96% and 87%, respectively ($p < 0.0001$ and 0.001 , Figure 3). Δ GTV-N ADC parameters at mid-RT, however, were not significantly associated with any of the studied endpoints ($P > 0.05$).

Univariable analysis of local control showed that GTV-P $\Delta\text{ADC}_{\text{mean}}$ at mid-RT $\geq 7\%$ was associated with improved LC (hazard ratio (HR), 0.06, 95% CI, 0.01–0.3, $p=0.001$). In a multivariable model that also included T-stage, smoking, and HPV status, GTV-P $\Delta\text{ADC}_{\text{mean}}$ at mid-RT remained statistically significant (HR, 0.03, 95% CI, 0.01–0.6, $p=0.02$) and achieved a better model performance as assessed using BIC criteria (BIC decrease = 19.8). After bootstrapping, the clinical LC model yielded a c-index of 0.77 ± 0.17 while the additive LC model (i.e., clinical + $\Delta\text{ADC}_{\text{mean}}$) yielded a c-index of 0.85 ± 0.16 which was significantly better than the clinical model ($p < 0.0001$).

Moreover, univariable analysis of recurrence-free survival showed that GTV-P $\Delta\text{ADC}_{\text{mean}}$ at mid-RT $\geq 7\%$ was associated with improved RFS (HR, 0.2, 95% CI, 0.06–0.6, $p=0.003$). In a multivariable model that also included age, AJCC 8th edition stage (i.e., which is based on T-stage, N-stage, tumor site and HPV-status data), and smoking status, GTV-P $\Delta\text{ADC}_{\text{mean}}$ at mid-RT remained statistically significant (HR, 0.3, 95% CI, 0.1–0.9, $p=0.04$) and also improved the model performance using BIC criteria (BIC decrease = 8). After bootstrapping, the clinical RFS model yielded a c-index of 0.68 ± 0.23 while the additive RFS model yielded a c-index of 0.74 ± 0.22 which also was significantly better than the clinical models ($p < 0.0001$).

Similarly, a univariable analysis of overall survival showed that GTV-P $\Delta\text{ADC}_{\text{mean}}$ at mid-RT $\geq 7\%$ was associated with improved OS (HR, 0.2, 95% CI, 0.04–0.9, $p=0.037$). However, it was not statistically significant when added to a multivariable clinical model.

The volumetric analysis showed that there was a significant decrease in mid-RT residual tumor volumes for both GTV-P and GTV-N compared to baseline pre-RT volumes (3.5 vs. 11.1 mm³ for GTV-P and 7.4 vs. 11.8 mm³ for GTV-N, $p < 0.0001$ for both). However, the mean Δ volume decrease at mid-RT was significantly higher in GTV-P compared with GTV-N (69% vs. 30%, $p < 0.0001$). As shown in Figure 4, there was no statistically significant correlation of the Δ volume and $\Delta\text{ADC}_{\text{mean}}$ for both GTV-P (Spearman's Rho = -0.06, $p=0.6$) and GTV-N (Spearman's Rho = -0.2, $p=0.1$). Δ volume changes were not significantly correlated with any endpoints ($P > 0.05$). Only baseline GTV-P volume (i.e., a surrogate of T-stage) was significantly correlated with LC on univariable analysis ($p=0.03$).

For ROI subvolume analysis, patients with mid-RT non-CR at the primary site had no statistically significant difference in all ADC parameters between GTV-P-RS and GTV-P-RD ($p > 0.05$ for all). RPA identified $\Delta\text{ADC}_{\text{mean}} < 5\%$ and $< 10\%$ as the strongest predictors of

local recurrence for GTV-P-RD and GTV-P-RS, respectively ($p=0.02$ for both). However, for RFS only $\Delta\text{ADC}_{\text{mean}} < 5\%$ for GTV-P-RD was significantly associated with worse RFS ($p=0.01$).

We retrospectively collected the images of 50 patients as an independent external validation dataset. Patients in this dataset were treated between August 2017 and September 2021. 92% were men and the median age was 64 years (range 46–86). A summary of patient demographic, disease, and treatment criteria is presented in Supplementary Table 1. All patients had gross GTV-P at baseline. The median follow-up time was 37 months (IQR, 16–49). The 2-year LC, RFS, and OS were 90%, 79%, and 92%, respectively. The total number of recurrence events was 11 (22%). Two, three, and three patients had an isolated local, regional, and distant recurrence events, respectively. One and two patients had combined local & distant and locoregional recurrences, respectively. The 2-Year LC and RFS for patients with $\Delta\text{ADC}_{\text{mean}} < 7\%$ compared to patients with $\geq 7\%$ at mid-RT were 74% and 30% versus 95% and 95%, respectively ($p=0.04$ and <0.0001 , Supplementary Figure 2). After bootstrapping, the clinical LC model yielded a c-index of 0.74 ± 0.20 while the additive LC model (i.e., clinical + $\Delta\text{ADC}_{\text{mean}}$) yielded a c-index of 0.78 ± 0.19 which was significantly better than the clinical model ($p < 0.0001$). Furthermore, the clinical RFS model yielded a c-index of 0.53 ± 0.24 while the additive RFS model yielded a c-index of 0.70 ± 0.21 which also was significantly better than the clinical models ($p < 0.0001$).

Discussion

Our results show that DWI changes during RT are a significant predictor of oncologic outcomes. The significant increase in mid-RT ADC parameters for both tumor and nodal ROIs reflects a decrease in cellular density in tumor tissue caused by the radiation effect that induces breakdown of cellular membranes which ultimately decrease the restriction of diffusion shown in baseline tumor tissue.[34–36] The increased diffusion in mid-RT images was successfully measured by the studied ADC parameters that showed a higher increase in patients who ultimately developed CR at the end of treatment compared to patients with residual disease.

Our study also identified an ADC biomarker of local control and recurrence-free survival using a GTV-P $\Delta\text{ADC}_{\text{mean}}$ threshold of 7% increase relative to baseline ADC_{mean} . These delta ADC changes were volume independent as our analysis methodology, illustrated in Figure 1, ensured that we use the same 3-D shape and volume of GTV-P propagated from baseline DWIs after image co-registration. We also assessed the effect of subvolume analysis within the subset of patients with non-CR at mid-RT images. In that subset, both $\Delta\text{ADC}_{\text{mean}}$ changes in the residual and responding subvolumes were significantly associated with local control with a 5% and 10% threshold of ADC_{mean} increase. The threshold is lower in residual volumes as expected because of the higher relative tissue density in these subvolumes. This also indicates that quantitative DWI parameter maps can detect the mesoscale cellular changes that could not be otherwise detected using gross visual assessment. Furthermore, this also shows that even within the apparent residual tumors on anatomic imaging at mid-RT, there is a subset that expresses higher ADC changes and those tend to have better LC and RFS. These changes during treatment can serve as a biomarker to predict outcomes and can also

be used as a biological tool to adapt therapy dose according to the predicted response during therapy.

An additional significant finding in our study is that pretreatment DWI parameters had no significant association with outcomes, indicating that dynamic information obtained from RT-induced imaging changes during treatment is likely more informative compared to baseline status. Several previous studies matched our findings of no association between pretreatment ADC and outcomes [20, 37, 38] while a prior pilot set from our group as well as other studies showed a significant correlation.[14, 39–41] We believe that pretreatment ADC parameters of a relatively homogenous cohort with a majority of HPV positive oropharyngeal cancer would be less predictive of outcomes when compared to a more heterogenous group of HNC subsites and/or tumor types. A heterogenous group of tumors will likely have a mixture of well and poorly differentiated tumors with different level of cellularity and stromal contents which thereby lead to more contrast in the degree of diffusion between different tumor types.[36] Therefore, we think that the pretreatment DWI parameters may be a more prognostic than predictive biomarker as it reflects the nature of the baseline tumor rather than predicting its response to therapy.[42]

According to the criteria set by the Biomarker Qualification Program (BQP) that was developed by the Center for Drug Evaluation and Research (CDER, US Food and Drug Administration), a qualified biomarker must be within a specified context of use (COU) that defines the BEST biomarker category and its intended use.[42–44] Our findings from this prospective observational imaging study suggest that the COU for $\Delta\text{ADC}_{\text{mean}}$ can be used as a response biomarker for defining HNC patients with high-risk of local failure according to their response to RT at an actionable mid-therapy time point. These results encourage us to apply for further full qualification package from the BQP with a properly defined COU. This will also allow a promising imaging biomarker like DWI to cross the second translational gap and eventually become a clinical decision-making tool according to the framework recommended by the imaging biomarker roadmap for cancer studies.[45]

In-treatment ΔADC were investigated in prior studies with relatively small sample sizes consisting of mixtures of HNC subsites, and in concordance with our results, these studies showed that ΔADC during RT was a significant correlate of oncologic outcomes.[11, 18, 37] To our knowledge, we present the largest prospective imaging study to date supporting that primary tumor ΔADC change during treatment is a strong biomarker of important oncologic outcomes, particularly for local control and recurrence-free survival. The threshold of ΔADC used should be carefully interpreted according to the nature of the primary tumor subsite, technique of segmentation/image registration, and DWI acquisition parameters (i.e., b values). Notably, ΔADC is a relative rather than an absolute value which could represent a more robust biomarker that is less susceptible to inter-patient and inter-scanner variability and thereby more clinically generalizable. In patients with mainly HPV positive oropharyngeal primary site using 3-D volumetric analysis of GTV-P at mid-RT relative to baseline, $\Delta\text{ADC}_{\text{mean}} < 7\%$ was shown to be a strong correlate of local failure.

However, our study is not without limitations. Importantly, our study utilized a single-institution cohort. However, we did both internal and external validation of our findings

with bootstrapping methods and independent testing of a separate dataset. We aim for further validation in the near future using multi-institutional datasets. Another limitation was the use of two DWI sequences during the study (i.e., BLADE and RESOLVE); however, after analyzing the ADC values extracted from both DWI sequences using the Kolmogorov-Smirnov test, no significant differences were found between the two sequences. Lastly, we failed to show any significant correlation between nodal DWI changes and regional control, which could potentially be attributed to the cystic nature of the studied GTV-Ns in our sample. As a future step, we plan to analyze these LNs using a morphologic distinction between solid and cystic component in each node rather than the standard segmentation approach.

In conclusion, our prospective imaging study of HNC patients demonstrated that Δ ADC parameters at mid-RT represent a strong predictor of local recurrence and recurrence-free survival. Patients with no significant increase of mid-RT ADC at the primary tumor site relative to baseline values are at high-risk of disease relapse. Multi-institutional data are needed for validation of our results.

Supplementary Material

Refer to Web version on PubMed Central for supplementary material.

Funding sources and financial disclosures:

Dr. Mohamed & Dr. Fuller received/receives funding and salary support from directly related to this project from: NIH National Institute of Dental and Craniofacial Research (NIDCR) Academic Industrial Partnership Grant (R01DE028290); NIDCR Establishing Outcome Measures for Clinical Studies of Oral and Craniofacial Diseases and Conditions award (R01DE025248); NIH/NSF NCI Smart Connected Health Program (R01CA257814). Dr. Fuller received/receives funding and salary support from directly unrelated to this project from: NCI Parent Research Project Grant (R01CA258827); NCI Ruth L. Kirschstein NRSA Institutional Research Training Grant (T32CA261856); NIH NIDCR Exploratory/Developmental Research Grant Program (R21DE031082); National Institutes of Health (NIH) National Cancer Institute (NCI) Early Stage Development of Technologies in Biomedical Computing, Informatics, and Big Data Science Program (R01CA214825); NSF/NIH Joint Initiative on Quantitative Approaches to Biomedical Big Data program (R01CA225190); NIH National Institute of Biomedical Imaging and Bioengineering (NIBIB) Research Education Programs for Residents and Clinical Fellows Grant (R25EB025787); NCI Early Phase Clinical Trials in Imaging and Image-Guided Interventions Program (1R01CA218148); NIH/NCI Cancer Center Support Grant (CCSG) Pilot Research Program Award from the UT MD Anderson CCSG Radiation Oncology and Cancer Imaging Program (P30CA016672); Small Business Innovation Research Grant Program a sub-award from Oncospace, Inc. (R43CA254559); The Human BioMolecular Atlas Program (HuBMAP) Integration, Visualization & Engagement (HIVE) Initiative (OT2OD026675) sub-award; Patient-Centered Outcomes Research Institute (PCS-1609-36195) sub-award from Princess Margaret Hospital; National Science Foundation (NSF) Division of Civil, Mechanical, and Manufacturing Innovation (CMMI) grant (NSF 1933369). Dr. Fuller receives grant and infrastructure support from MD Anderson Cancer Center via: the Charles and Daneen Stiefel Center for Head and Neck Cancer Oropharyngeal Cancer Research Program; the Program in Image-guided Cancer Therapy; and the NIH/NCI Cancer Center Support Grant (CCSG) Radiation Oncology and Cancer Imaging Program (P30CA016672). Dr. Fuller has received direct industry grant/in-kind support, honoraria, and travel funding from Elekta AB. TCS was supported by The University of Texas Health Science Center at Houston Center for Clinical and Translational Sciences TL1 Program (TL1 TR003169). Dr. Lai receives funding and salary support from R01DE025248, R01DE028290, R21CA259839, NRG-HN006, and T32CA261856.

References

- [1]. Perri F, Ionna F, Muto P, Marzo MD, Caponigro F, Longo F, et al. Genetics and management of locally advanced carcinomas of the head and neck: role of altered fractionation radiotherapy. *Future Sci OA*. 2018;5:FSO347-FSO.

- [2]. Ang KK, Harris J, Wheeler R, Weber R, Rosenthal DI, Nguyen-Tan PF, et al. Human papillomavirus and survival of patients with oropharyngeal cancer. *The New England journal of medicine*. 2010;363:24–35. [PubMed: 20530316]
- [3]. Dahlstrom KR, Calzada G, Hanby JD, Garden AS, Glisson BS, Li G, et al. An evolution in demographics, treatment, and outcomes of oropharyngeal cancer at a major cancer center: a staging system in need of repair. *Cancer*. 2013;119:81–9. [PubMed: 22736261]
- [4]. Garden AS, Kies MS, Morrison WH, Weber RS, Frank SJ, Glisson BS, et al. Outcomes and patterns of care of patients with locally advanced oropharyngeal carcinoma treated in the early 21st century. *Radiat Oncol*. 2013;8:21. [PubMed: 23360540]
- [5]. Sandulache VC, Hamblin J, Lai S, Pezzi T, Skinner HD, Khan NA, et al. Oropharyngeal squamous cell carcinoma in the veteran population: Association with traditional carcinogen exposure and poor clinical outcomes. *Head Neck*. 2015;37:1246–53. [PubMed: 24801106]
- [6]. Kontaxis C, Bol GH, Lagendijk JJ, Raaymakers BW. Towards adaptive IMRT sequencing for the MRlinac. *Physics in medicine and biology*. 2015;60:2493–509. [PubMed: 25749856]
- [7]. Kontaxis C, Bol GH, Lagendijk JJ, Raaymakers BW. A new methodology for inter- and intrafraction plan adaptation for the MR-linac. *Physics in medicine and biology*. 2015;60:7485–97. [PubMed: 26371425]
- [8]. Bostel T, Nicolay NH, Grossmann JG, Mohr A, Delorme S, Echner G, et al. MR-guidance-- a clinical study to evaluate a shuttle- based MR-linac connection to provide MR-guided radiotherapy. *Radiat Oncol*. 2014;9:12. [PubMed: 24401489]
- [9]. Vandecaveye V, De Keyzer F, Nuyts S, Deraedt K, Dirix P, Hamaekers P, et al. Detection of head and neck squamous cell carcinoma with diffusion weighted MRI after (chemo)radiotherapy: correlation between radiologic and histopathologic findings. *Int J Radiat Oncol Biol Phys*. 2007;67:960–71. [PubMed: 17141979]
- [10]. Kim S, Loevner L, Quon H, Sherman E, Weinstein G, Kilger A, et al. Diffusion-weighted magnetic resonance imaging for predicting and detecting early response to chemoradiation therapy of squamous cell carcinomas of the head and neck. *Clin Cancer Res*. 2009;15:986–94. [PubMed: 19188170]
- [11]. Vandecaveye V, Dirix P, De Keyzer F, de Beeck KO, Vander Poorten V, Roebben I, et al. Predictive value of diffusion-weighted magnetic resonance imaging during chemoradiotherapy for head and neck squamous cell carcinoma. *Eur Radiol*. 2010;20:1703–14. [PubMed: 20179939]
- [12]. Ryoo I, Kim JH, Choi SH, Sohn CH, Kim SC. Squamous Cell Carcinoma of the Head and Neck: Comparison of Diffusion-weighted MRI at b-values of 1,000 and 2,000 s/mm² to Predict Response to Induction Chemotherapy. *Magnetic resonance in medical sciences : MRMS : an official journal of Japan Society of Magnetic Resonance in Medicine*. 2015;14:337–45. [PubMed: 26104081]
- [13]. Chen Y, Liu X, Zheng D, Xu L, Hong L, Xu Y, et al. Diffusion-weighted magnetic resonance imaging for early response assessment of chemoradiotherapy in patients with nasopharyngeal carcinoma. *Magnetic resonance imaging*. 2014;32:630–7. [PubMed: 24703576]
- [14]. Ng SH, Lin CY, Chan SC, Lin YC, Yen TC, Liao CT, et al. Clinical utility of multimodality imaging with dynamic contrast-enhanced MRI, diffusion-weighted MRI, and 18F-FDG PET/CT for the prediction of neck control in oropharyngeal or hypopharyngeal squamous cell carcinoma treated with chemoradiation. *PloS one*. 2014;9:e115933.
- [15]. Noij DP, Pouwels PJ, Ljumanovic R, Knol DL, Doornaert P, de Bree R, et al. Predictive value of diffusion-weighted imaging without and with including contrast-enhanced magnetic resonance imaging in image analysis of head and neck squamous cell carcinoma. *European journal of radiology*. 2015;84:108–16. [PubMed: 25467228]
- [16]. Hoang JK, Choudhury KR, Chang J, Craciunescu OI, Yoo DS, Brizel DM. Diffusion-weighted imaging for head and neck squamous cell carcinoma: quantifying repeatability to understand early treatment-induced change. *AJR American journal of roentgenology*. 2014;203:1104–8. [PubMed: 25341151]
- [17]. Lambrecht M, Van Calster B, Vandecaveye V, De Keyzer F, Roebben I, Hermans R, et al. Integrating pretreatment diffusion weighted MRI into a multivariable prognostic model for head and neck squamous cell carcinoma. *Radiotherapy and oncology : journal of the European Society for Therapeutic Radiology and Oncology*. 2014;110:429–34. [PubMed: 24630535]

- [18]. Matoba M, Tuji H, Shimode Y, Toyoda I, Kuginuki Y, Miwa K, et al. Fractional change in apparent diffusion coefficient as an imaging biomarker for predicting treatment response in head and neck cancer treated with chemoradiotherapy. *AJNR American journal of neuroradiology*. 2014;35:379–85. [PubMed: 24029391]
- [19]. Hong J, Yao Y, Zhang Y, Tang T, Zhang H, Bao D, et al. Value of magnetic resonance diffusion-weighted imaging for the prediction of radiosensitivity in nasopharyngeal carcinoma. *Otolaryngology--head and neck surgery : official journal of American Academy of Otolaryngology-Head and Neck Surgery*. 2013;149:707–13. [PubMed: 23884282]
- [20]. Chawla S, Kim S, Dougherty L, Wang S, Loevner LA, Quon H, et al. Pretreatment diffusion-weighted and dynamic contrast-enhanced MRI for prediction of local treatment response in squamous cell carcinomas of the head and neck. *AJR American journal of roentgenology*. 2013;200:35–43. [PubMed: 23255739]
- [21]. Vandecaveye V, Dirix P, De Keyzer F, Op de Beeck K, Vander Poorten V, Hauben E, et al. Diffusion-weighted magnetic resonance imaging early after chemoradiotherapy to monitor treatment response in head-and-neck squamous cell carcinoma. *Int J Radiat Oncol Biol Phys*. 2012;82:1098–107. [PubMed: 21514067]
- [22]. Ding Y, Hazle JD, Mohamed AS, Frank SJ, Hobbs BP, Colen RR, et al. Intravoxel incoherent motion imaging kinetics during chemoradiotherapy for human papillomavirus-associated squamous cell carcinoma of the oropharynx: preliminary results from a prospective pilot study. *NMR in biomedicine*. 2015;28:1645–54. [PubMed: 26451969]
- [23]. Lambrecht M, Van Herck H, De Keyzer F, Vandecaveye V, Slagmolen P, Suetens P, et al. Redefining the target early during treatment. Can we visualize regional differences within the target volume using sequential diffusion weighted MRI? *Radiotherapy and oncology : journal of the European Society for Therapeutic Radiology and Oncology*. 2014;110:329–34. [PubMed: 24231234]
- [24]. Hauser T, Essig M, Jensen A, Gerigk L, Laun FB, Munter M, et al. Characterization and therapy monitoring of head and neck carcinomas using diffusion-imaging-based intravoxel incoherent motion parameters-preliminary results. *Neuroradiology*. 2013;55:527–36. [PubMed: 23417120]
- [25]. Campbell SR, Mohamed AS, Heukelom J, Awan MJ, Garden AS, Gunn GB, et al. Primary Tumor Regression Index: The Prognostic Value of Volumetric Image Guided Radiation Therapy for Head and Neck Cancer. *Int J Radiat Oncol Biol Phys*. 2016;96:E363–e4.
- [26]. Ding Y, Mohamed ASR, Yang J, Colen RR, Frank SJ, Wang J, et al. Prospective observer and software-based assessment of magnetic resonance imaging quality in head and neck cancer: Should standard positioning and immobilization be required for radiation therapy applications? *Practical Radiation Oncology*. 2015;5:e299–e308. [PubMed: 25544553]
- [27]. Ding Y, Meheissen MAM, Zhou K, Mohamed ASR, Wen Z, Ng SP, et al. Evaluation of different diffusion-weighted image techniques for head and neck radiation treatment: phantom and volunteer studies. *medRxiv*. 2022:2022.03.22.22272705.
- [28]. Naser MA, Wahid KA, Ahmed S, Salama V, Dede C, Edwards BW, et al. Quality assurance assessment of intra-acquisition diffusion-weighted and T2-weighted magnetic resonance imaging registration and contour propagation for head and neck cancer radiotherapy. *Medical physics*. 2022.
- [29]. van Dijk LV, Wahid KA, Ahmed S, Elgohari B, McCoy L, Sharafi SC, et al. Big Data Statistical Learning Improves Survival Prediction For Head And Neck Cancer Patients. *International Journal of Radiation Oncology, Biology, Physics*. 2020;108:e796–e7.
- [30]. Volinsky CT, Raftery AE. Bayesian information criterion for censored survival models. *Biometrics*. 2000;56:256–62. [PubMed: 10783804]
- [31]. Raftery AE. Bayesian model selection in social research. *Sociological methodology*. 1995:111–63.
- [32]. Pölsterl S. scikit-survival: A Library for Time-to-Event Analysis Built on Top of scikit-learn. *J Mach Learn Res*. 2020;21:1–6. [PubMed: 34305477]
- [33]. Altman DG, McShane LM, Sauerbrei W, Taube SE. Reporting recommendations for tumor marker prognostic studies (REMARK): explanation and elaboration. *BMC Medicine*. 2012;10:51. [PubMed: 22642691]

- [34]. Baliyan V, Das CJ, Sharma R, Gupta AK. Diffusion weighted imaging: Technique and applications. *World J Radiol.* 2016;8:785–98. [PubMed: 27721941]
- [35]. Chung SR, Choi YJ, Suh CH, Lee JH, Baek JH. Diffusion-weighted Magnetic Resonance Imaging for Predicting Response to Chemoradiation Therapy for Head and Neck Squamous Cell Carcinoma: A Systematic Review. *Korean journal of radiology.* 2019;20:649–61. [PubMed: 30887747]
- [36]. King AD, Thoeny HC. Functional MRI for the prediction of treatment response in head and neck squamous cell carcinoma: potential and limitations. *Cancer Imaging.* 2016;16:23-. [PubMed: 27542718]
- [37]. King AD, Mo FK, Yu KH, Yeung DK, Zhou H, Bhatia KS, et al. Squamous cell carcinoma of the head and neck: diffusion-weighted MR imaging for prediction and monitoring of treatment response. *Eur Radiol.* 2010;20:2213–20. [PubMed: 20309553]
- [38]. Ng SH, Lin CY, Chan SC, Yen TC, Liao CT, Chang JT, et al. Dynamic contrast-enhanced MR imaging predicts local control in oropharyngeal or hypopharyngeal squamous cell carcinoma treated with chemoradiotherapy. *PloS one.* 2013;8:e72230.
- [39]. Ohnishi K, Shioyama Y, Hatakenaka M, Nakamura K, Abe K, Yoshiura T, et al. Prediction of local failures with a combination of pretreatment tumor volume and apparent diffusion coefficient in patients treated with definitive radiotherapy for hypopharyngeal or oropharyngeal squamous cell carcinoma. *Journal of radiation research.* 2011;52:522–30. [PubMed: 21905311]
- [40]. Hatakenaka M, Nakamura K, Yabuuchi H, Shioyama Y, Matsuo Y, Ohnishi K, et al. Pretreatment apparent diffusion coefficient of the primary lesion correlates with local failure in head-and-neck cancer treated with chemoradiotherapy or radiotherapy. *Int J Radiat Oncol Biol Phys.* 2011;81:339–45. [PubMed: 20832179]
- [41]. Ding Y, Fuller C, Mohamed A, Frank S, Rosenthal D, Colen R, et al. Intravoxel Incoherent Motion Magnetic Resonance Imaging of Oropharyngeal Cancer in Response to Chemoradiation Therapy. *International Journal of Radiation Oncology, Biology, Physics.* 2014;90:S75.
- [42]. Amur S, LaVange L, Zineh I, Buckman-Garner S, Woodcock J. Biomarker Qualification: Toward a Multiple Stakeholder Framework for Biomarker Development, Regulatory Acceptance, and Utilization. *Clinical pharmacology and therapeutics.* 2015;98:34–46. [PubMed: 25868461]
- [43]. Amur SG, Sanyal S, Chakravarty AG, Noone MH, Kaiser J, McCune S, et al. Building a roadmap to biomarker qualification: challenges and opportunities. *Biomarkers in medicine.* 2015;9:1095–105. [PubMed: 26526897]
- [44]. Group F-NBW. BEST (Biomarkers, endpoints, and other tools) resource [Internet]. 2016.
- [45]. O'Connor JPB, Aboagye EO, Adams JE, Aerts HJWL, Barrington SF, Beer AJ, et al. Imaging biomarker roadmap for cancer studies. *Nature Reviews Clinical Oncology.* 2017;14:169–86.

Highlights

- Patients with CR had a significant increase in ADC_{mean} at mid-RT.
- Primary tumor $\Delta ADC_{mean} < 7\%$ at mid-RT was associated with worse LC and RFS.
- Multivariable analysis showed ΔADC_{mean} at mid-RT $\geq 7\%$ was associated with better outcomes.
- The addition of ΔADC_{mean} improved the c-indices of LC and RFS prediction models.
- Primary tumor ΔADC at mid-RT is a response biomarker for high-risk local failure.

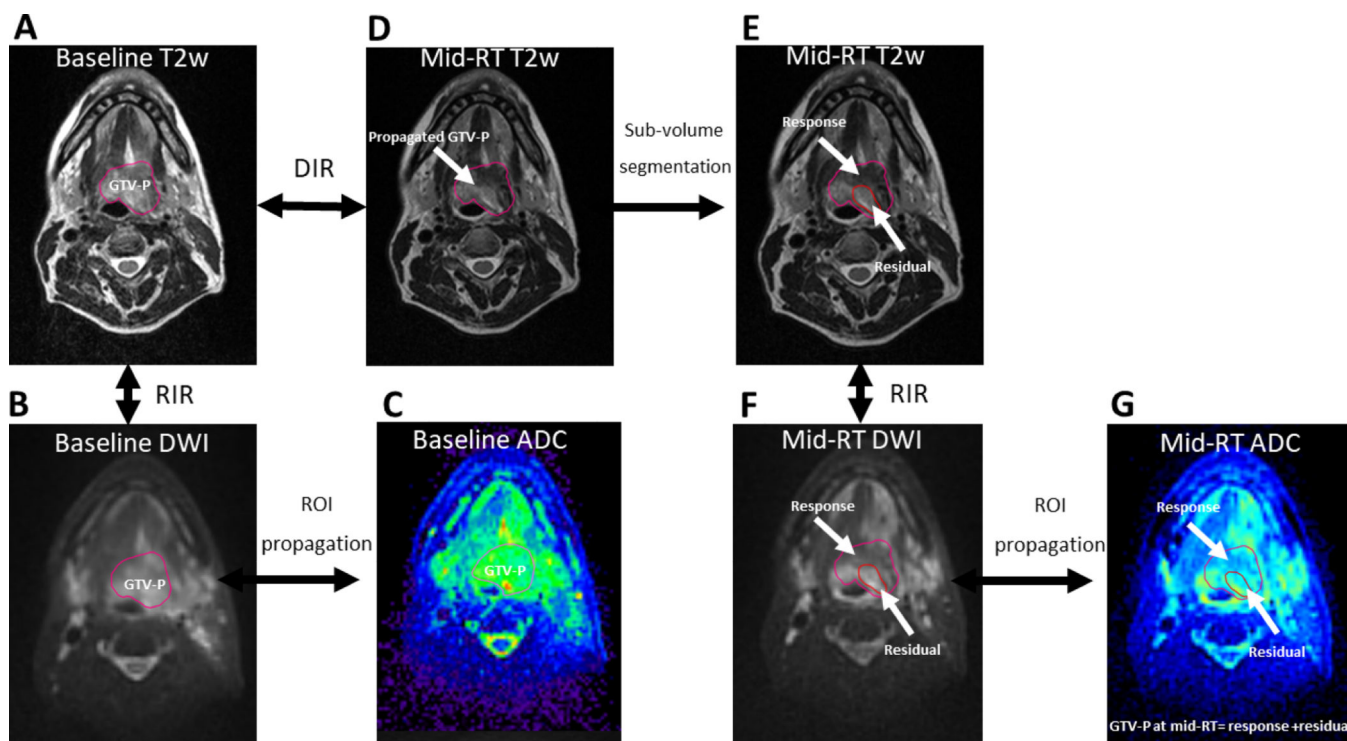


Figure 1. Image registration and segmentation workflow
 Illustration of the workflow process for image registration and segmentation in the study using an example of a patient with T4N1 tumor of the base of tongue. Panel (A) shows the GTV-P segmentation on baseline T2w MRI followed by rigid co-registration (RIR) and contour propagation to baseline DWI (B) and then ROI propagation to corresponding ADC map (C). Panel (D) shows mid-RT T2w image with partial response. The image was co-registered to baseline T2w using deformable image registration (DIR) and baseline GTV-P was propagated. Subsequently, the residual and response sub-volumes were segmented (E), then contours were propagated to mid-RT DWI after RIR (F), and finally to the corresponding mid-RT ADC map (G).

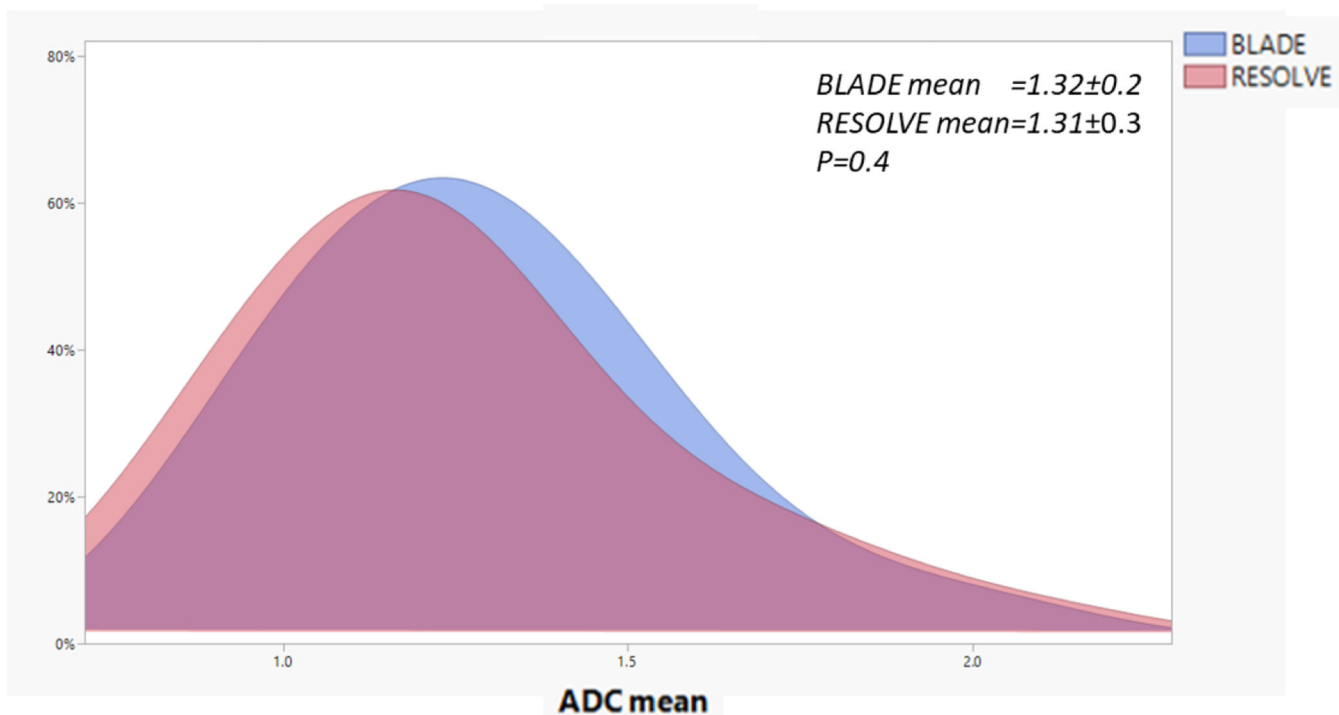


Figure 2. BLADE vs. RESOLVE histograms. Histogram illustration of the distribution of tumor and nodal volumes' ADC mean at baseline using the BLADE vs. RESOLVE DWI acquisition methods in the study. The RESOLVE in pink is overlaid on BLADE in light blue. There were no statistically significant differences using the Kolmogorov–Smirnov test ($p=0.4$).

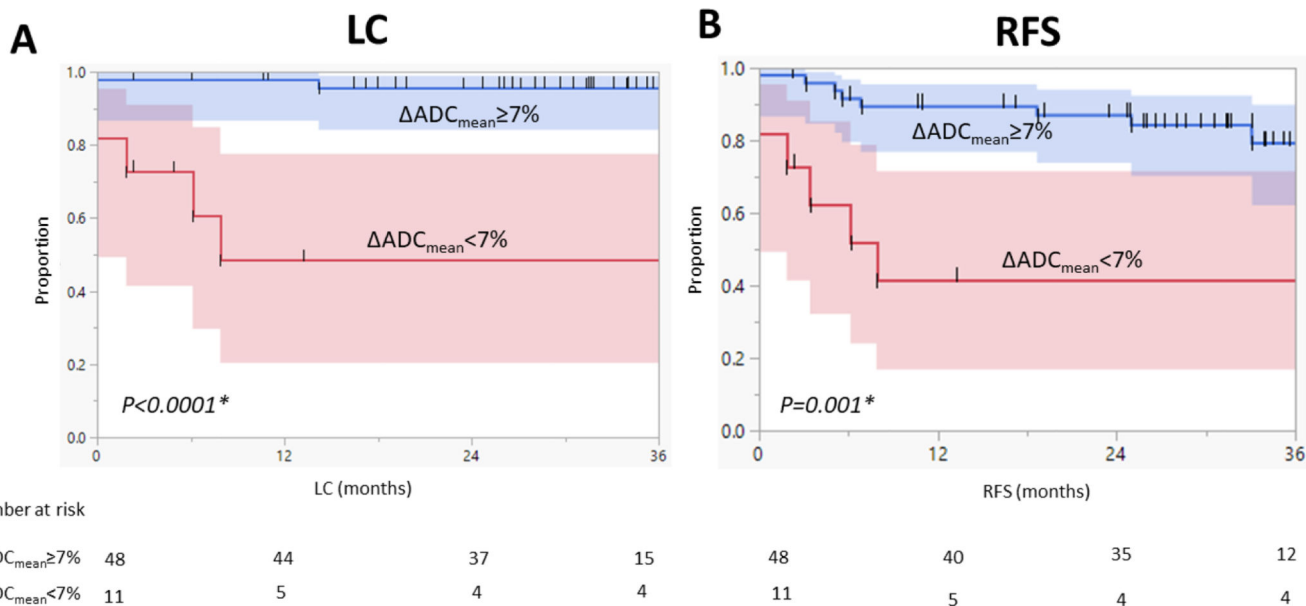


Figure 3. Kaplan–Meier curves calculated for patients with baseline GTV-P (n = 59) show better (A) local control (LC) and (B) recurrence-free survival (RFS) for patients with $\geq 7\%$ ΔADC_{mean} at mid-RT. Shaded colors represent 95% confidence intervals, short vertical lines represent censored data, and asterisks indicate significant log-rank p values.

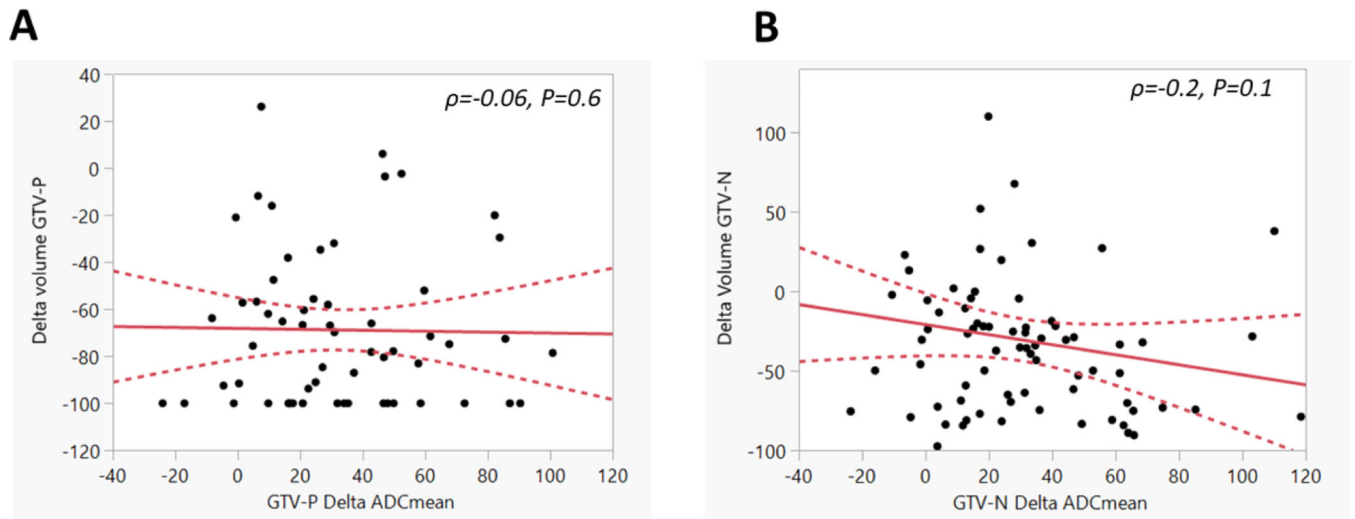


Figure 4. Relationship between Δ volume and Δ ADC_{mean} for both GTV-P (A) and GTV-N (B) at mid-RT. Solid lines represent the linear fit and dotted lines represent the 95% confidence intervals.

Table 1.

Patient demographic, disease, and treatment characteristics.

Characteristic	Patients No. (%)
Age (years)	
median (range)	61 (33–78)
Sex	
Male	75 (93)
Female	6 (7)
Smoking status	
Never	37 (46)
Former	35 (43)
Current	9 (11)
Smoking pack-year	
mean (SD)	15 (26)
Disease subsite	
Base of tongue	29 (36)
Tonsil	38 (47)
CUP	12 (15)
Others	2 (2)
T stage	
T0	12 (15)
Tx	6 (7)
T1	13 (16)
T2	24 (30)
T3	9 (11)
T4	17 (21)
N stage	
N0	6 (7)
N1	42 (52)
N2	31(38)
N3	2 (3)
AJCC 8thed. Stage	
I	38 (47)
II	20 (25)
III	17 (21)
IVa	6 (7)
HPV status	
Positive	73 (90)
Negative	8 (10)
Radiation Dose	
Mean in Gy (SD)	69.6 (1.3)
Radiation Fractions	

Characteristic	Patients No. (%)
Mean (SD)	33 (0.9)
Radiation technique	
IMRT/VMAT	55 (68)
IMPT	26 (32)
Chemotherapy	
None	16 (20)
Induction	1 (1)
Concurrent with RT	54 (67)
Induction + Concurrent	10 (12)

Abbreviations: CUP, carcinoma of unknown primary; SD, standard deviation; Gy, Gray; IMRT, intensity-modulated radiotherapy; VMAT, Volumetric Modulated Arc Therapy; IMPT, intensity modulated proton therapy.

Author Manuscript

Author Manuscript

Author Manuscript

Author Manuscript

Table 2.

ADC parameter changes at mid-RT versus baseline values.

ADC parameter (x10 ⁻³ mm ² /s)	End-RT response	Baseline GTV-P	Mid-RT GTV-P	P value	Baseline GTV-N	Mid-RT GTV-N	P value
ADC Mean	CR	1.37±0.2	1.8±0.3	<0.0001	1.27±0.3	1.6±0.4	<0.0001
	Non-CR	1.3±0.2	1.6±0.4	0.07	1.28±0.3	1.54±0.3	0.01
ADC 5th percentile	CR	0.87±0.3	1.2±0.3	<0.0001	0.76±0.2	1.04±0.3	<0.0001
	Non-CR	1.1±0.6	1.3±0.5	0.4	1.02±0.4	1.19±0.3	0.2
ADC 10th percentile	CR	0.97±0.3	1.32±0.3	<0.0001	0.86±0.2	1.16±0.3	<0.0001
	Non-CR	1.2±0.5	1.42±0.4	0.3	1.06±0.3	1.26±0.2	0.02
ADC 20th percentile	CR	1.1±0.3	1.47±0.3	<0.0001	0.97±0.3	1.3±0.4	<0.0001
	Non-CR	1.2±0.4	1.47±0.3	0.4	1.11±0.3	1.34±0.2	0.01
ADC 30th percentile	CR	1.17±0.3	1.58±0.3	<0.0001	1.06±0.3	1.4±0.4	<0.0001
	Non-CR	1.2±0.3	1.5±0.3	0.3	1.16±0.2	1.4±0.1	0.009
ADC 40th percentile	CR	1.25±0.3	1.68±0.3	<0.0001	1.14±0.3	1.5±0.4	<0.0001
	Non-CR	1.22±0.3	1.56±0.3	0.	1.21±0.2	1.45±0.2	0.01
ADC Median	CR	1.35±0.2	1.8±0.3	<0.0001	1.22±0.3	1.58±0.4	<0.0001
	Non-CR	1.25±0.2	1.6±0.2	0.07	1.25±0.3	1.51±0.2	0.009
ADC 60th percentile	CR	1.42±0.3	1.9±0.4	<0.0001	1.32±0.4	1.67±0.4	<0.0001
	Non-CR	1.3±0.2	1.68±0.5	0.1	1.3±0.3	1.57±0.3	0.009
ADC 70th percentile	CR	1.52±0.3	1.95±0.4	<0.0001	1.43±0.4	1.78±0.5	<0.0001
	Non-CR	1.36±0.3	1.7±0.6	0.1	1.36±0.4	1.64±0.4	0.009
ADC 80th percentile	CR	1.6±0.3	2.1±0.4	<0.0001	1.57±0.4	1.91±0.5	<0.0001
	Non-CR	1.4±0.3	1.8±0.7	0.07	1.45±0.4	1.72±0.5	0.01
ADC 90th percentile	CR	1.79±0.4	2.22±0.4	<0.0001	1.76±0.4	2.07±0.5	<0.0001
	Non-CR	1.52±0.4	1.99±0.8	0.03	1.57±0.5	1.84±0.6	0.1
ADC 95th percentile	CR	1.9±0.4	2.36±0.5	<0.0001	1.93±0.4	2.2±0.5	<0.0001
	Non-CR	1.61±0.6	2.09±0.9	0.03	1.65±0.7	1.97±0.8	0.1

Author Manuscript

Author Manuscript

Author Manuscript

Author Manuscript